Check for updates

View Article Online
View Journal

ChemComm
Chemical Communications

Accepted Manuscript

This article can be cited before page numbers have been issued, to do this please use: Y. Gao, X. Guo, B. Xie, J. Miao, Y. Zou and C. Yang, *Chem. Commun.*, 2026, DOI: 10.1039/D6CC00501B.

This is an Accepted Manuscript, which has been through the Royal Society of Chemistry peer review process and has been accepted for publication.

Accepted Manuscripts are published online shortly after acceptance, before technical editing, formatting and proof reading. Using this free service, authors can make their results available to the community, in citable form, before we publish the edited article. We will replace this Accepted Manuscript with the edited and formatted Advance Article as soon as it is available.

You can find more information about Accepted Manuscripts in the Information for Authors.

Please note that technical editing may introduce minor changes to the text and/or graphics, which may alter content. The journal's standard Terms & Conditions and the Ethical guidelines still apply. In no event shall the Royal Society of Chemistry be held responsible for any errors or omissions in this Accepted Manuscript or any consequences arising from the use of any information it contains.

ROYAL SOCIETY OF CHEMISTRY

rsc.li/chemcomm

Please do not adjust margins

ChemComm

View Article Online
DOI: 10.1039/D6CC00501B

COMMUNICATION

Open Access Article. Published on 31 March 2026. Downloaded on 4/2/2026 10:46:59 AM.
This article is licensed under a Creative Commons Attribution-NonCommercial 3.0 Unported Licence.

Triazatruxene Decorated Multi-Resonance Emitter with Hybrid Short- and Long-Range Charge-Transfer Excited States Enables Efficient Narrowband Deep-Blue Electroluminescence

Received 00th January 20xx,
Accepted 00th January 20xx

DOI: 10.1039/x0xx00000x

Ying Gao,[a,b+] Xiaoyu Guo,[a+] Bingjie Xie,[a] Jingsheng Miao,[a] Yang Zou,[a*] Chuluo Yang[a*]

A TADF emitter with hybrid short- and long-range charge-transfer excited states is designed by grafting the triazatruxene donor onto the multi-resonance framework. The emitter exhibits narrowband deep-blue emission with enhanced photophysical properties and enables efficient deep-blue electroluminescence.

Thermally activated delayed fluorescence (TADF) materials enable high electroluminescence efficiency without noble metals.[1] Conventional donor–acceptor (D–A) TADF emitters effectively reduce the singlet–triplet energy gap (ΔE_{ST}) to promote reverse intersystem crossing (RISC), but their long-range charge-transfer (LR-CT) character often leads to broad emission and poor color-purity, limiting deep-blue OLED applications. To address this issue, the multiple-resonance (MR) strategy introduced by Hatakeyama et al. employs rigid, planar frameworks with atomically defined donor and acceptor units, producing short-range charge-transfer (SR-CT) excited states and narrowband emission.[2, 3] However, the highly localized electronic structures of MR-TADF emitters generally result in slow RISC rates (k_{RISC}), causing incomplete triplet harvesting and efficiency loss.[4, 5] According to Fermi's golden rule, k_{RISC} can be enhanced by reducing ΔE_{ST} or increasing spin–orbit coupling (SOC),[6] yet ΔE_{ST} reduction in MR systems is intrinsically limited. While heavy-atom incorporation enhances SOC,[7-9] it may compromise stability.[10, 11] Alternatively, boron-based MR frameworks can introduce a "hidden" LR-CT state, providing a heavy-atom-free route to accelerate k_{RISC} and achieve high-efficiency, color-pure OLEDs.[12-16]

As one of the primary colors, deep-blue emission plays a critical role in next-generation display technologies.[17] The MR framework BNO, composed of carbazole and phenol as resonant partners, is a well-established building block for deep-blue emitters.[18, 19] Despite its intrinsic narrowband deep-blue emission, BNO-based MR emitters typically suffer from moderate photoluminescence quantum yields (PLQYs) and slow k_{RISC}, which result in limited device efficiency and pronounced efficiency roll-off in electroluminescent devices. To address these limitations, we sought to accelerate k_{RISC} in BNO-based MR emitters by introducing additional LR-CT excited states. Accordingly, a series of MR-TADF emitters—BNO-DPAC, BNO-DMAC, and BNO-tBuDMAC were designed by decorating the BNO MR moiety with acridine-based donors (**Scheme 1**).[20] Systematic investigation revealed that the donor structure exerts a profound influence on the photophysical properties. **BNO-DPAC**, featuring a quasi-axial acridine conformation, exhibits the weakest LR-CT character, thereby retaining

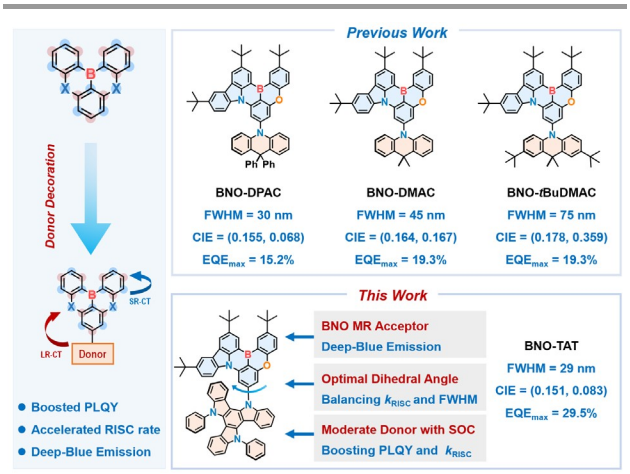

Scheme 1. Chemical structures and molecular design of the BNO-based emitters.

[a] Shenzhen Key Laboratory of New Information Display and Storage Materials, College of Materials Science and Engineering, Shenzhen University, Shenzhen 518060, China. Shenzhen 518060, PR China
[b] College of Physics and Optoelectronic Engineering, Shenzhen University, Shenzhen 518060, People's Republic of China
+ These authors contributed equally to this work
†Supplementary Information available: [Experimental section, related spectra of the materials; TGA and electrochemistry curves, electroluminesence data]. See DOI: 10.1039/x0xx00000x

ChemComm Accepted Manuscript

Please do not adjust margins

View Article Online
DOI: 10.1039/D6CC00501B

Open Access Article. Published on 31 March 2026. Downloaded on 4/2/2026 10:46:59 AM.
This article is licensed under a Creative Commons Attribution-NonCommercial 3.0 Unported Licence.

narrowband deep-blue emission but suffering from the low PLQY and slow k_{RISC}. In contrast, the stronger donors in BNO-DMAC and BNO-tBuDMAC significantly enhance PLQY and k_{RISC} but induce pronounced red shifts and spectral broadening, deviating from the desired deep-blue region. These results highlight the critical yet challenging requirement of precisely balancing donor strength to activate LR-CT-assisted RISC while preserving narrowband deep-blue emission originating from SR-CT states.

Triazatruxene (TAT) is a well-established donor motif in D–A-type TADF emitters, known for its high PLQY and fast k_{RISC}.[21-23] We proposed TAT as an ideal donor for BNO-based emitters with coexisting short- and long-range charge-transfer (SR/LR-CT) excited states, aiming to achieve narrowband deep-blue emission, high PLQY, and accelerated k_{RISC} simultaneously. This design is supported by the moderate electron-donating strength of TAT, comparable to DMAC, and its unique C_{3h}-symmetric double indolo[3,2-b]carbazole framework, which reduces the D–A twisting angle and enables well-regulated LR-CT character. Moreover, the triarylamine-rich structure facilitates the formation of multiple CT excited states with enhanced spin–orbit coupling, providing additional pathways for triplet harvesting. Based on this strategy, a BNO-TAT emitter was synthesized, exhibiting a significantly accelerated k_{RISC}. Sensitizer-free OLEDs based on BNO-TAT achieved efficient deep-blue emission with preserved color purity and an EQE approaching 30%, nearly double that of BNO-DPAC-based control device.

The chemical structure of the designed emitter namely **BNO-TAT** is shown in **Scheme 1**, along with the **BNO-DPAC** as the control emitter. The BNO acceptor moiety was prepared *via* sequential nucleophilic substitution and borylation reactions. Subsequently, the TAT and the acceptor fragment were coupled through a Buchwald-Hartwig amination to afford the target product **BNO-TAT** (**Scheme S1**). Its chemical structure was unambiguously confirmed by ^{1}H NMR, ^{13}C NMR, 2D COSY and ROESY NMR spectroscopies and high-resolution mass spectrometry (**Fig. S1**-**S6**, supplementary information). Moreover, thermogravimetric analysis (TGA, **Fig. S7**) revealed a thermal decomposition temperature of 490 °C for **BNO-TAT**, demonstrating excellent thermal stability and confirming its suitability for vacuum thermal evaporation in device fabrication.

To further elucidate the rationality of the molecular design, density functional theory (DFT) and time-dependent DFT (TD-DFT) calculations were carried out using the Gaussian 16 software package with the B3LYP functional. As depicted in **Fig. 1** and **Fig. S9-S11**, the highest occupied molecular orbital (HOMO) is primarily localized on the TAT donor, while the lowest unoccupied molecular orbital (LUMO) resides on the MR-type acceptor fragment, confirming the intended D-A electronic separation. The calculated dihedral angle between the donor and acceptor units is 69.5°, which is close to that of the single crystal structure, and consistent with the design objective of achieving a well-regulated LR-CT character. Natural transition orbital (NTO) analysis reveals that both **BNO-TAT** and **BNO-DPAC** exhibit pronounced LR-CT character in their S_1 states,

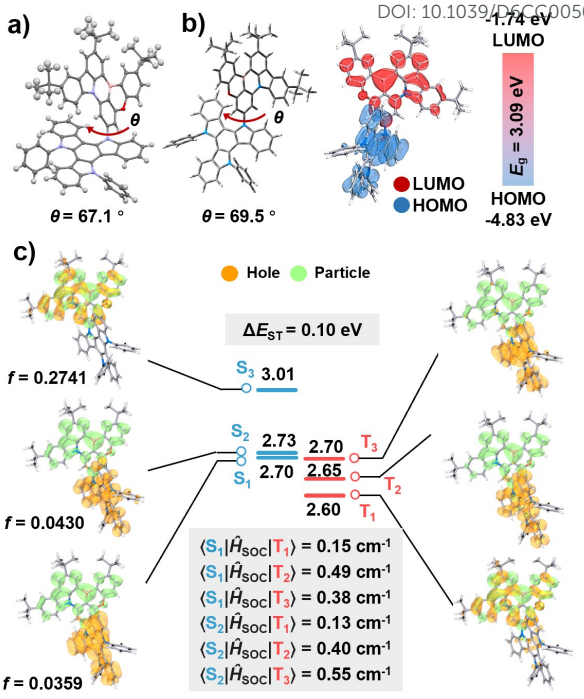

Fig. 1 a) Crystal structure (CCDC: 2536739), b) optimized molecular structure, FMOs distribution, c) related state energy energies, NTO distribution and SOCMEs of **BNO-TAT** acquired from the theoretical calculation.

accompanied by several closely lying higher singlet (S_n) states with SR-CT character within an energy window of 0.30 eV.

Although the two emitters possess comparable T_1 energies, the stronger electron-donating ability of TAT stabilizes the S_1 state of **BNO-TAT**, resulting in a reduced singlet-triplet energy gap (ΔE_{ST}) of 0.10 eV, approximately half that of **BNO-DPAC** (0.24 eV), indicative of enhanced TADF behavior. Notably, **BNO-TAT** exhibits a significantly denser manifold of singlet and triplet excited states than **BNO-DPAC (Fig. S11)**, with four nearly degenerate singlet and triplet states distributed within 0.08 eV. This dense excited-state landscape facilitates multiple triplet exciton upconversion pathways, thereby enhancing exciton utilization efficiency in the electroluminescence (EL) devices. Furthermore, NTO analysis of the T_1-T_3 states reveal hybrid SR/LR-CT character, with greater spatial overlap between hole and particle distributions in the S_n and T_n states of **BNO-TAT** compared to **BNO-DPAC**. Such NTOs lead to markedly enhanced spin-orbit coupling matrix elements (SOCMEs) of 0.49 and 0.38 cm^{-1} for $\langle S_1|\hat{H}_{SOC}|T_2\rangle$and $\langle S_1|\hat{H}_{SOC}|T_3\rangle$, respectively. These values are substantially higher than those of **BNO-DPAC** (0.04 and 0.09 cm^{-1}, **Fig. S5**). In addition, the oscillator strength of the S_1 state in **BNO-TAT** (f = 0.0359) is nearly an order of magnitude larger than that of **BNO-DPAC** (f = 0.0032), consistent with its higher PLQY. Collectively, these computational results provide strong theoretical support for the superior photophysical and electroluminescent performance of **BNO-TAT**.

The absorption, fluorescence (Fl.), and phosphorescence (Phos.) spectra of **BNO-TAT** were measured in a dilute toluene solution. As shown in **Fig. 2a and Fig. S12**, **BNO-TAT** exhibits

ChemComm Accepted Manuscript

 This journal is © The Royal Society of Chemistry 20xx

View Article Online
DOI: 10.1039/D6CC00501B

Open Access Article. Published on 31 March 2026. Downloaded on 4/2/2026 10:46:59 AM.
This article is licensed under a Creative Commons Attribution-NonCommercial 3.0 Unported Licence.

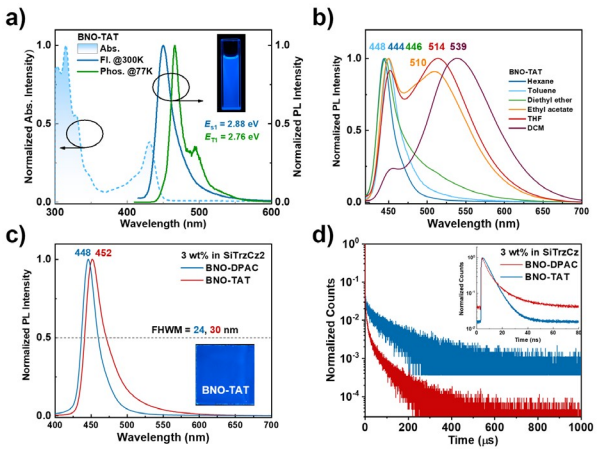

Fig. 2 a) UV-vis absorption, fluorescence at 300K and phosphorescence spectra at 77K in toluene ($1.0*10^{-5}$ M); b) solvatochromic effect on photoluminescent (PL) spectra for **BNO-TAT**; c) PL spectra of the emitters in SiTrzCz2 host; d) Transient PL decay curves of emitters in SiTrzCz2 at 300K

strong broadband absorption in the range of 300-370 nm, primarily attributed to π-π* and n-π* transitions of the arylamine and BNO moieties. The intense primary absorption band centered at 430 nm is assigned to the SR-CT-type transitions from the MR-type acceptor. In a dilute toluene solution, **BNO-TAT** exhibits an emission maximum at 450 nm with a full width at half maximum (FWHM) of only 26 nm, indicating a negligible spectral shift compared to **BNO-DPAC**. This spectral similarity underlies achieving high-purity deep-blue electroluminescence in OLEDs. Moreover, based on the onset of fluorescence and phosphorescence spectra, the ΔE_{ST} for **BNO-TAT** is calculated to be only 0.12 eV, indicating its TADF character.

Beyond the intrinsic narrowband deep-blue emission arising from the SR-CT excited state, solvatochromic studies were performed to elucidate the presence of a hidden LR-CT character. As shown in **Fig. 2b**, **BNO-TAT** exhibits a dominant sharp emission peak at approximately 450 nm in low- to medium-polarity solvents (hexane and toluene), which is characteristic of SR-CT fluorescence. Upon increasing the solvent polarity, a weak tailing emission beyond 500 nm emerges in diethyl ether. Notably, in more polar solvents, **BNO-TAT** displays a clear dual-emission behavior: the narrow emission centered at ~450 nm remains essentially unchanged with increasing polarity, confirming its SR-CT origin, while a broad emission band undergoes a pronounced bathochromic shift from 510 nm in ethyl acetate to 514 nm in tetrahydrofuran and ultimately becomes the dominant peak at 539 nm in dichloromethane. This pronounced solvatochromic response provides direct evidence for the involvement of LR-CT excited states in **BNO-TAT**, thereby validating the proposed molecular design strategy. In contrast, the reference compound **BNO-DPAC** exhibits only a weak shoulder around 530 nm even in highly polar dichloromethane,[20] indicating a much less pronounced LR-CT contribution. This comparison highlights the strengthened LR-CT character in **BNO-TAT**, which is expected to underpin its enhanced photophysical performance.

When doped into 9,9′-(6-(3-(triphenylsilyl)phenyl)-1,3,5-triazine-2,4-diyl)bis(9H-carbazole) (SiTrzCz2) at a concentration of 3 wt%, both emitters exhibit strong photoluminescence, achieving PLQYs of 99% for **BNO-TAT** and 92% for **BNO-DPAC**. As shown in **Fig. 2c**, the doped films display emission maxima at 448 nm for **BNO-TAT** and 452 nm for **BNO-DPAC**, respectively. Compared to their emissions in dilute toluene solutions, both materials show slight red shifts and moderate spectral broadening, which can be attributed to π-π interactions with the host matrix. Notably, in contrast to the previously reported **BNO-DMAC**, which exhibits a significantly broadened emission (FWHM = 56 nm) due to excessive LR-CT character, **BNO-TAT** maintains a much narrower emission bandwidth (FWHM = 30 nm) due to ideal hybrid SR/LR-CT character. This well-preserved narrowband deep-blue emission is critical for achieving high color purity in display applications.

Transient photoluminescence decay measurements were conducted to evaluate the TADF characteristics of both emitters. As illustrated in **Fig. 2d**, **BNO-TAT** exhibits a longer prompt fluorescence lifetime (τ_p = 10.0 ns) than **BNO-DPAC** (τ_p = 6.1 ns), consistent with its enhanced LR-CT character. **BNO-TAT** shows a pronounced temperature dependence (**Fig. S13**), with a delayed fluorescence lifetime of 28.4±0.2 μs and a delayed component contribution of approximately 68%, indicative of dominant TADF behavior. In contrast, **BNO-DPAC** exhibits a longer delayed lifetime of 66.2±0.2 μs, and lower delayed component contributes of 52%. Benefiting from its well-regulated LR-CT character, **BNO-TAT** not only achieves near-unity PLQY but also exhibits an accelerated k_{RISC} of 1.1×10^5 s^{-1}, over three times that of **BNO-DPAC** (**Table S1**). These results provide compelling evidence for more efficient triplet exciton utilization, underscoring the advantages of this design strategy for high-performance OLED applications.

OLEDs were fabricated to evaluate the electroluminescent performance of the two emitters, employing the following layer structure: indium tin oxide (ITO)/1,4,5,8,9-hexaazatriphenylene-hexacarbonitrile (HATCN, 5 nm)/1,1-

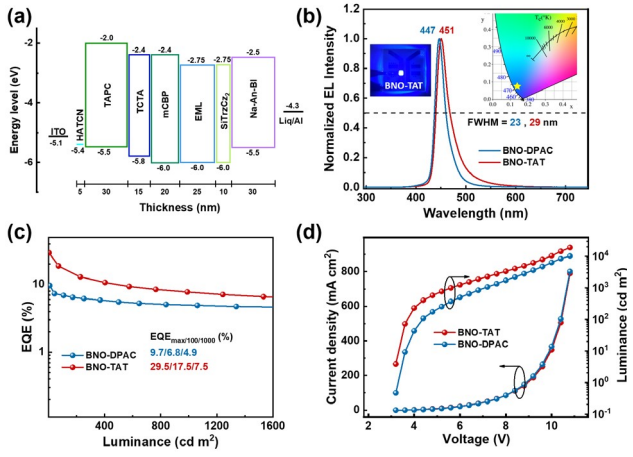

Fig. 3 a) Device configuration and the energy level diagrams; b) EL spectra (inset: images of EL device); c) EQE versus luminance curves; d) current density and luminance versus voltage (*J-V-L*) characteristics of the doped devices.

ChemComm Accepted Manuscript

View Article Online
DOI: 10.1039/D5CC05019B

Open Access Article. Published on 31 March 2026. Downloaded on 4/2/2026 10:46:59 AM. This article is licensed under a Creative Commons Attribution-NonCommercial 3.0 Unported Licence.

bis[(di-4-tolylamino)-phenyl]cyclohexane (TAPC, 30 nm)/tris(4-carbazol-9-ylphenyl)amine (TCTA, 15 nm)/1,3-di(9*H*-carbazol-9-yl)benzene (mCBP, 20 nm)/emissive layer (EML, 25 nm)/9,9'-(6-(4-(triphenylsilyl)phenyl)-1,3,5-triazine-2,4-diyl)bis(9*H*-carbazole) (SiTrzCz2, 10 nm)/2-ethyl-1-(4-(10-(naphthalen-2-yl)anthracen-9-yl)phenyl)-1H-benzo[d]imidazole (Na-An-BI, 30 nm)/lithium quinolate (Liq, 2 nm)/aluminum (Al, 100 nm). In this structure, TAPC and Na-An-BI function as hole-transport and electron-transport layers, respectively, while mCBP serves as both a hole-blocking and exciton-confining layer. HATCN acts as an anode interfacial layer, and Liq serves as a cathode interfacial layer. Given the HOMO energy level of the emitter at -5.12 eV, the EML was adopted with a doping system of SiTrzCz2: 1 wt%, 3 wt%, 5 wt%, 7 wt% **BNO-TAT** and 3 wt% **BNO-DPAC**, where SiTrzCz2 is used as the host material. The chemical structures of the materials used in the EL device are shown in **Fig. S14.**

As shown in **Fig. 3** and **Fig. S15-S17,** summarized in **Table S2**, at a doping concentration of 1 wt%, the **BNO-TAT**-based device displayed a narrowband deep-blue emission peaked at 448 nm and a FHWM of 28 nm, corresponding to the Commission Internationale de l'Éclairage (CIE) chromaticity coordinates of (0.156, 0.069). Aside from the well-maintained narrowband deep-blue emission, the maximum external quantum efficiency (EQE_{max}) and maximum brightness (L_{max}) reached 25.8% and 15780 cd m^{-2}, these values are significantly superior than others BNO-based emitters reported in the literature.[18-20] At the doping concentration of 3 wt%, **BNO-TAT** delivered further optimized performance: with stable emission peaked at 446 nm and FWHM of 29 nm. The EL peak positions closely match those of the corresponding PL spectra of the doped films. The EQE_{max} reaches up to 30%, representing a twofold enhancement compared to the control device using **BNO-DPAC** as the emitter, while the peak brightness achieves 18916 cd m^{-2}, which is nearly double that of the **BNO-DPAC**-based device. These much superior electroluminescent characteristics can be attributed to the intrinsically high PLQY of **BNO-TAT** and the efficient utilization of triplet excitons enabled by its TADF mechanism.

In conclusion, by decorating a triazatruxene donor onto a BNO MR framework, we have developed an emitter that features hybrid SR/LR-CT excited states. The well-regulated LR-CT character introduced by the triazatruxene unit preserves the intrinsic narrowband deep-blue emission and high PLQY of the MR moiety, while enabling enhanced photophysical properties through a dense manifold of excited states that facilitates more efficient triplet exciton utilization. As a result, the emitter exhibits a high PLQY together with accelerated k_{RISC} without sacrificing spectral narrowness in the deep-blue region. Consequently, doped OLEDs based on this emitter achieve a EQE_{max} of 29.5% while maintaining narrowband deep-blue emission, representing a highly competitive performance among state-of-the-art deep-blue emitters.

Acknowledgements

We gratefully acknowledge financial support from the National Natural Science Foundation of China (52573203 and 52130308), Guangdong Basic and Applied Basic Research Foundation (2025A1515010777), the Shenzhen Science and Technology Program (ZDSYS20210623091813040 and JCYJ20250604182224032), Research Team Cultivation Program of Shenzhen University (2023DFT004). We also thank the Instrumental Analysis Center of Shenzhen University for analytical support.

Conflicts of interest

There are no conflicts to declare.

Data availability

The data supporting this article have been included as part of the ESI.

Notes and references

1 Y. Liu, C. Li, Z. Ren, S. Yan and M. R. Bryce, *Nat. Rev. Mater.*, 2018, **3**, 18020.
2 T. Hatakeyama, K. Shiren, K. Nakajima, S. Nomura, S. Nakatsuka, K. Kinoshita, J. Ni, Y. Ono and T. Ikuta, *Adv. Mater.*, 2016, **28**, 2777-2781.
3 Y. Kondo, K. Yoshiura, S. Kitera, H. Nishi, S. Oda, H. Gotoh, Y. Sasada, M. Yanai and T. Hatakeyama, *Nat.Photonics*, 2019, **13**, 678-682.
4 X. Wu, S. Ni, C. H. Wang, W. Zhu and P. T. Chou, *Chem. Rev.*, 2025, **125**, 6685-6752.
5 M. Mamada, M. Hayakawa, J. Ochi and T. Hatakeyama, *Chem. Soc. Rev.*, 2024, **53**, 1624-1692.
6 P. K. Samanta, D. Kim, V. Coropceanu and J.-L. Brédas, *J. Am. Chem. Soc.*, 2017, **139**, 4042-4051.
7 Y. X. Hu, J. Miao, T. Hua, Z. Huang, Y. Qi, Y. Zou, Y. Qiu, H. Xia, H. Liu, X. Cao and C. Yang, *Nat. Photonics*, 2022, **16**, 803-810.
8 I. S. Park, H. Min and T. Yasuda, *Angew. Chem. Int. Ed.*, 2022, **61**, e202205684.
9 H. Lin, Z. Ye, S. Xian, Z. Chen, J. Miao, Z. Huang, C. Zhong, S. Gong, X. Cao and C. Yang, *Adv Mater*, 2025, **37**, e2502459.
10 J. Liu, J. Miao, J. Dong, Z. Chen, Z. Huang and C. Yang, *Adv. Mater.*, 2026, **38**, e13987.
11 Y. Zou, M. Yu, Y. Xu, Z. Xiao, X. Song, Y. Hu, Z. Xu, C. Zhong, J. He, X. Cao, K. Li, J. Miao and C. Yang, *Chem*, 2024, **10**, 1485-1501.
12 J. Han, Y. Chen, N. Li, Z. Huang and C. Yang, *Aggregate*, 2022, **3**, e182.
13 Y. Xu, C. Li, Z. Li, Q. Wang, X. Cai, J. Wei and Y. Wang, *Angew. Chem. Int. Ed.*, 2020, **59**, 17442-17446.
14 S. Liao, Z. Zhang, Y. Gao, Z. Chen, J. Miao, Y. Zou and C. Yang, *Chin. J. Chem.* 2025, **44**, 303-310.
15 Y.-H. He, J.-Y. Liu, Z. Zhang, G.-W. Chen, Y.-C. Wang, G. Yuan, F.-M. Xie, J.-X. Tang and Y.-Q. Li, *Matter*, 2025, **8**.
16 Z. Huang, H. Xie, J. Miao, Y. Wei, Y. Zou, T. Hua, X. Cao and C. Yang, *J. Am. Chem. So.c*, 2023, **145**, 12550-12560.
17 A. Monkman, *ACS Appl. Mater. Interfaces*, 2022, **14**, 20463-20467.
18 J. Han, Z. Huang, X. Lv, J. Miao, Y. Qiu, X. Cao and C. Yang, *Adv. Opt. Mater.*, 2021, **10**, 2102092.
19 J. Park, J. Lim, J. H. Lee, B. Jang, J. H. Han, S. S. Yoon and J. Y. Lee, *ACS Appl. Mater. Interfaces*, 2021, **13**, 45798-45805.
20 X. Huang, Y. Xu, J. Miao, Y.-Y. Jing, S. Wang, Z. Ye, Z. Huang, X. Cao and C. Yang, *J. Mater. Chem. C*, 2023, **11**, 11885-11894.
21 P. L. Dos Santos, J. S. Ward, D. G. Congrave, A. S. Batsanov, J. Eng, J. E. Stacey, T. J. Penfold, A. P. Monkman and M. R. Bryce, *Adv. Sci.*, 2018, **5**, 1700989.

ChemComm Accepted Manuscript

 This journal is © The Royal Society of Chemistry 20xx

Please do not adjust margins

View Article Online
DOI: 10.1039/D6CC00501B

22 D. H. Ahn, S. W. Kim, H. Lee, I. J. Ko, D. Karthik, J. Y. Lee and J. H. Kwon, *Nat. Photonics*, 2019, **13**, 540.
23 K. R. Naveen, H. Lee, R. Braveenth, D. Karthik, K. J. Yang, S. J. Hwang and J. H. Kwon, *Adv. Funct. Mater.*, 2021, **32**, 2110356.

Open Access Article. Published on 31 March 2026. Downloaded on 4/2/2026 10:46:59 AM.
This article is licensed under a Creative Commons Attribution-NonCommercial 3.0 Unported Licence.

ChemComm Accepted Manuscript

Please do not adjust margins

The data supporting this article have been included as part of the Supplementary Information.

View Article Online
DOI: 10.1039/D6CC00501B

Open Access Article. Published on 31 March 2026. Downloaded on 4/2/2026 10:46:59 AM.
This article is licensed under a Creative Commons Attribution-NonCommercial 3.0 Unported Licence.

ChemComm Accepted Manuscript